Engineering Research Journal
journal homepage: https://erj.journals.ekb.eg/

Seismic Response of Box Girder Bridge Columns to Forward-Directivity and Fling-Step Ground Motions

Waleed Abdallah [1], Ahmed Abdelhamid Soliman [1,*], Magdy M.M. Genidi [1]

[1] Helwan University - Faculty of Engineering Mataria branch - Department of civil Engineering - Egypt

[*]Corresponding author E-mail: civil.ahss@gmail.com

Abstract.

Until recently, seismic design codes were generally based on research addressing far-field earthquake characteristics. However, with the increasing in recording the near-fault ground motions, it has been realized that special considerations should be considered for bridges located in near-fault regions. Several studies have investigated how the unique characteristics of near-fault motions, such as forward-directivity and fling-step, influence the seismic response and damage to concrete structures. The objective of this research was to investigate the effects of near-fault ground motions on the columns of box girder concrete bridges. To accomplish these goals, two and three spans of reinforced concrete bridges having box girder deck slab system using different columns height were developed in CSI-BRIDGE software package through three-dimensional nonlinear finite element models and subjected to fourteen types of near-fault records with pulse and characteristics representing forward-directivity and fling-step effects using nonlinear time-history analysis. The results showed that seismic inputs related to fling-step and forward-directivity effects greatly increase the seismic demands on the substructure elements in the longitudinal direction. Furthermore, the simulations reveal a significant impact of column height and number of spans on the seismic response of the bridge. The study found that records with a fling-step effect have a more pronounced effect on the seismic response of columns for the box girder bridges, especially at columns with the greater heights. In addition, reducing the number of spans amplifies the disparity between fling-step and forward-directivity responses. For models subjected to forward-directivity records, column responses increase with a higher PGV/PGA ratio. Furthermore, the increased response under fling-step motions is attributed to the presence of distinct pulses in both the acceleration and velocity time histories.

Keywords: Forward-directivity, Fling-step, RC bridges, Near fault earthquake motions,

DOI: 10.21608/erj.2025.339578.1145
Received 27 November 2024; Received in revised form 21 May 2025; Accepted 24 June 2025
Available online 01 September 2025

1. Introduction

Near-fault earthquakes generate unique challenges to structural design due to their intense and impulsive ground motions. Unlike far-fault earthquakes, near-fault events are characterized by forward directivity and fling-step effects, which can significantly increase structural demand. These effects are particularly pronounced within 20 kilometers of an active fault [1].

Design guidelines such as AASHTO and Caltrans have recognized the need for special considerations of structures located near faults. AASHTO requires site-specific analyses for bridges within 10 kilometers, while Caltrans recommends modifying the design spectra for sites within 25 kilometers. Considering the construction of bridges in these regions, ensuring their seismic performance under near-fault conditions is crucial for safety and resilience.

Past earthquakes have underscored the vulnerability of structures to near-fault ground motions. The 1994 Northridge earthquake in California highlighted the susceptibility of structures in the near-fault region to these intense events. Following the 1995 Kobe earthquake, Kawashima et al. (1998) documented the collapse of over 100 reinforced concrete bridge columns, demonstrating significant structural damage. The 1999 Kocaeli, Duzce, and Chi-Chi earthquakes provided further evidence of the destructive potential of near-fault ground motions. [2].

A primary factor contributing to this damage is the presence of velocity pulses within near-fault earthquakes. These pulses, unlike those in far-fault events, induce long-period responses in structures, leading to excessive deformation and potential failure [3, 4, 5].

Velocity pulses are classified into two types: forward-directivity and fling-step. Forward-directivity pulses are characterized by two-sided motion and do not cause permanent ground displacement. on the other hand, Fling-step pulses have a one-sided shape and result in permanent static ground displacement [6]. The specific characteristics of earthquakes occurring in near-fault regions, particularly fling-step and forward directivity, can lead to considerable damage to nearby structures. Consequently, these effects must be carefully evaluated, particularly for infrastructure.

To mitigate the risks associated with near-fault earthquakes, it is essential to incorporate these effects into structural design and analysis. This includes careful consideration of time history and dynamic analysis. By understanding and addressing the unique characteristics of near-fault ground motions, engineers can enhance the resilience of structures and protect public safety.

Liao et al. (2004) [7] conducted a comparative study on a concrete box girder bridge subjected to both near-fault and far-fault ground motions. Four bridge models were analyzed: two with seismic isolation and two without, each with varying pier heights to assess the response of short-period and intermediate-period piers. The goal was to evaluate the differential impact of near-fault and far-fault

earthquakes on bridge structures. The 1999 Chi-Chi Taiwan earthquake record was used to represent near-fault ground motions in the longitudinal direction of the bridge. The study found that near-fault ground motions resulted in significantly higher base shear forces and longitudinal displacements for all bridge configurations.

Chen et al. (2019) [8] conducted a comprehensive analysis of tall pier bridges subjected to near-fault conditions. Their study utilized analytical models calibrated through shake table experiments. In related research, the seismic response of continuous rigid-frame bridges was examined using selected near-fault records. The findings revealed a notable increase in structural response when exposed to pulse-like ground motions compared to non-pulse-like events [9].

Mahmoud et al. (2021) [10] investigated the influence of floor systems on building behavior during near-fault earthquakes with forward directivity and fling-step effects. Their findings revealed that buildings subjected to fling-step earthquakes experienced substantially greater seismic demands compared to those exposed to forward directivity events.

Xin L, Li X, Zhang Z, Zhao L (2019) [11] analyzed the seismic response of a long-span concrete-filled steel tubular arch bridge under three distinct ground motion categories, notably including records with fling-step, to enhance our understanding of their impact.

Li J, Xu LH (2023) [12] The study has revealed that continuous rigid-frame bridges are much more sensitive to near-fault ground shaking that includes velocity pulses.

Current design codes for reinforced concrete (RC) bridges are primarily developed based on seismic demands from far-fault earthquakes (typically beyond 20 km from the fault). However, their applicability to near-fault (NF) events remains uncertain. The considerable damage sustained by bridges located near fault ruptures during the 1994 Northridge (USA), 1999 Chi-Chi (Taiwan), and 1999 Kocaeli and Düzce (Turkey) earthquakes highlights this concern. Given that NF earthquakes can impose significantly higher seismic demands, further research into the seismic performance of bridges under such conditions is crucial for improving and updating existing design provisions.

The primary objective of this research is to examine the behavior and seismic response of reinforced concrete (RC) box girder bridges subjected to near-fault ground motions, specifically those exhibiting forward-directivity and fling-step effects. Understanding how these bridges respond to such distinct ground motion characteristics is crucial for enhancing structural design, improving public safety, and guiding appropriate structural choices in near-fault regions. Fling-step and forward-directivity ground motions impose different responses and velocity demands on structures, and recognizing these differences is essential to minimizing the risk of unexpected damage or failure during seismic events.

2. Materials Characteristics

2.1. Materials Characteristics for Concrete and steel

Adhering to the Egyptian Code of Practice (ECP 203) [13], the concrete compressive cube strength (Fcu) for both the superstructure and substructure components is established at 40 MPa. The concrete cylinder strength (Fc') is 32 MPa. Poisson's ratio is assigned to a value of 0.2. The tensile strength is approximately 3.80 MPa, and the elastic modulus (Ec) is 27828 MPa.

Steel bars used for reinforcing concrete elements in this analysis have a yield strength of 360 MPa for both main and transverse reinforcement. The modulus of elasticity for these steel reinforcement bars is 200000 MPa.

Figure 1 depicts the material models for concrete and steel as implemented in the CSI-Bridge software used in this study.

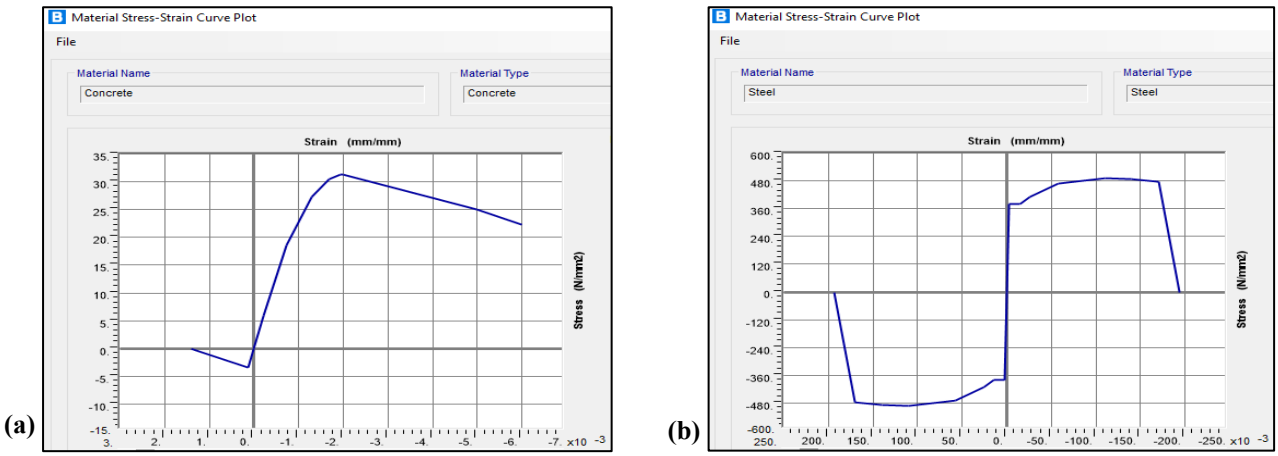

Fig 1 Stress-strain relation for (a) concrete and (b) steel

The concrete model (Fig. 1(a)) simulates its stress-strain response in both compressive and tensile states. Compressive behavior is characterized by a parabolic function up to the designated strength, followed by a softening region leading to failure. The steel model (Fig. 1(b)) exhibits linear elastic behavior under both tensile and compressive loads up to the yield limit. Subsequently, it shows strain hardening, where strain increases with continued stress until ultimate strength is achieved.

2.2. Materials Characteristics for Bearings

The superstructure of the bridge is supported by elastomeric bearings at each abutment. These bearings enable the bridge to move in the longitudinal direction, up to the maximum allowable shear deformation of the elastomer. The isolation system is represented in the bridge model using a link element with defined stiffness values as per the supplier guidelines.

3. Bridge Modeling and Methodology

3.1. Bridge configuration

Figures 2 and 3 illustrate schematic two-dimensional views of the bridge models analyzed in this study, representing typical two-span and three-span configurations of the constructed bridge in Damanhur City, located in the northern region of Egypt. The bridge was designed in 2014 and completed prior to mid-2017, in accordance with the Egyptian Code for reinforced concrete bridges [13]. To investigate the impact of forward directivity and fling step effects, six bridge models have been developed representing the box-girder bridge with column heights vary from 12.0 to 9.0 m using the CSI-BRIDGE software package [14]. The models are divided into two groups with two and three-spans as shown in figures 2 and 3. The bridge deck slab is a box-girder with cross sections as shown in figure 4,5 and 6. The bridges are supported by intermediate monolithic columns and two edge abutments. The longitudinal reinforcement ratio of the columns is 2.26% of the gross cross-sectional area. The volumetric reinforcement ratio of the spiral reinforcement is 0.8%. The concrete dimensions of typical designed columns and abutments are provided in Fig. 7 and 8. The superstructure rests on elastomeric bearings at the abutments and is fixed with the columns. The columns and abutments are supported on deep foundations with 1.0 m diameter of bearing piles capped by 1.75m and 1.50m pile caps at columns and abutments respectively. The boundary conditions of foundations are illustrated in figure 9.

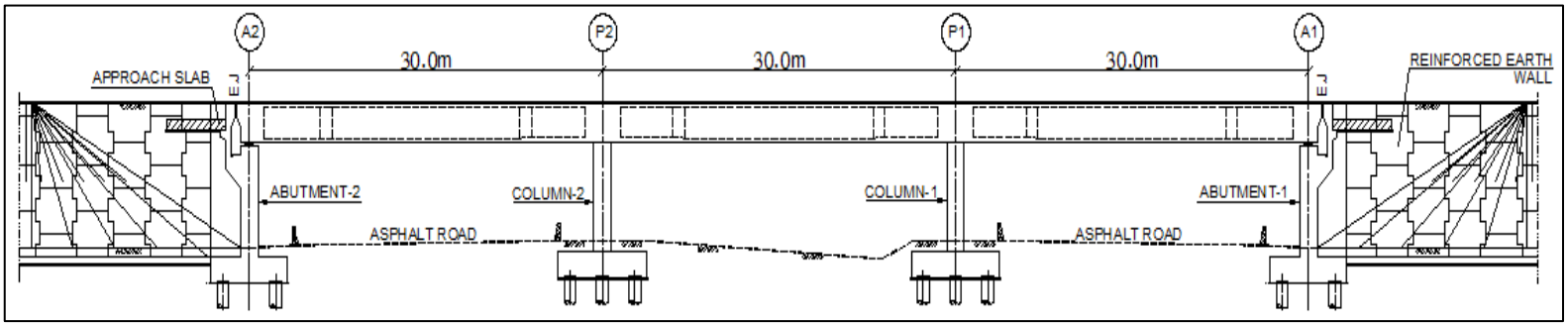

Fig 2 Longitudinal-sections of the considered box-girder bridge with three spans of 30m each

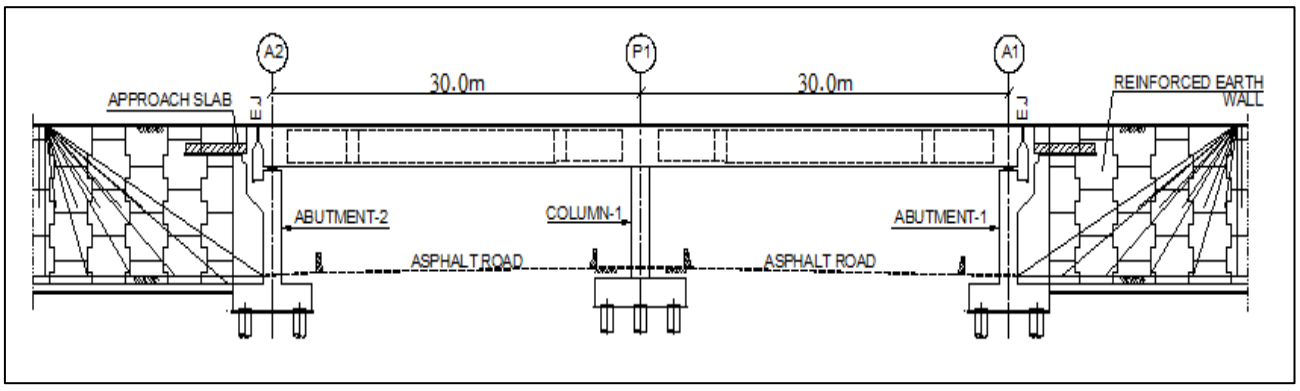

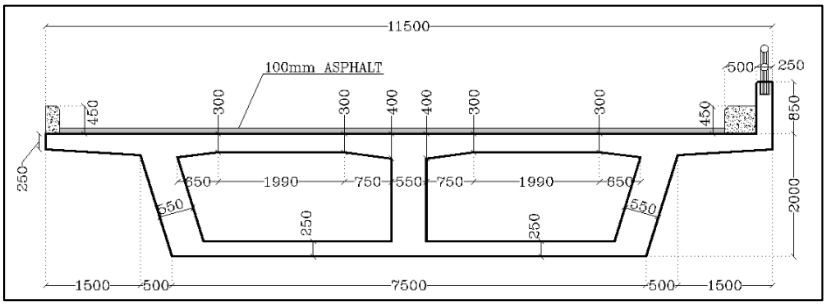

Fig 4 Cross section of box-girder bridge - Over abutments section

Fig 3 sections of the considered box-girder bridge with two spans of 30m each

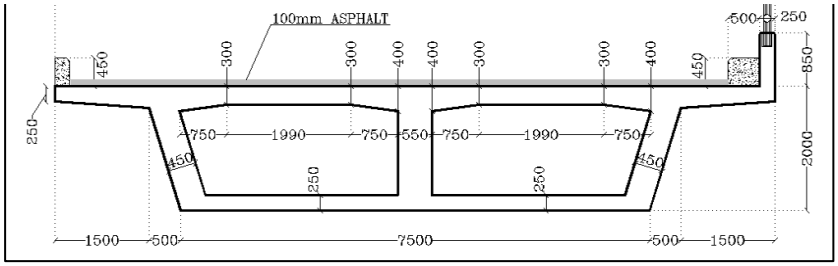

Fig 5 Cross section of box-girder bridge - Middle section

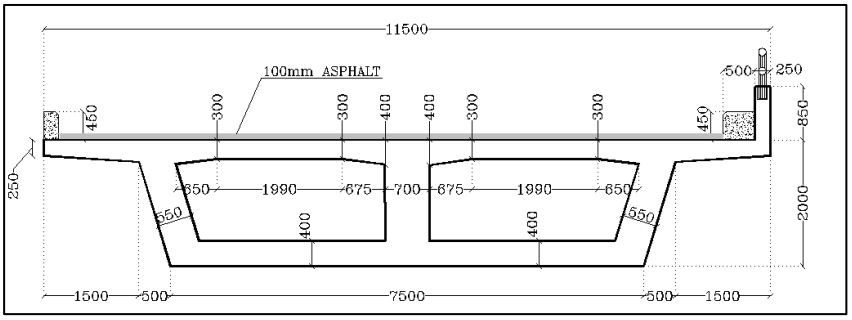

Fig 6 Cross section of box-girder bridge - Over columns section

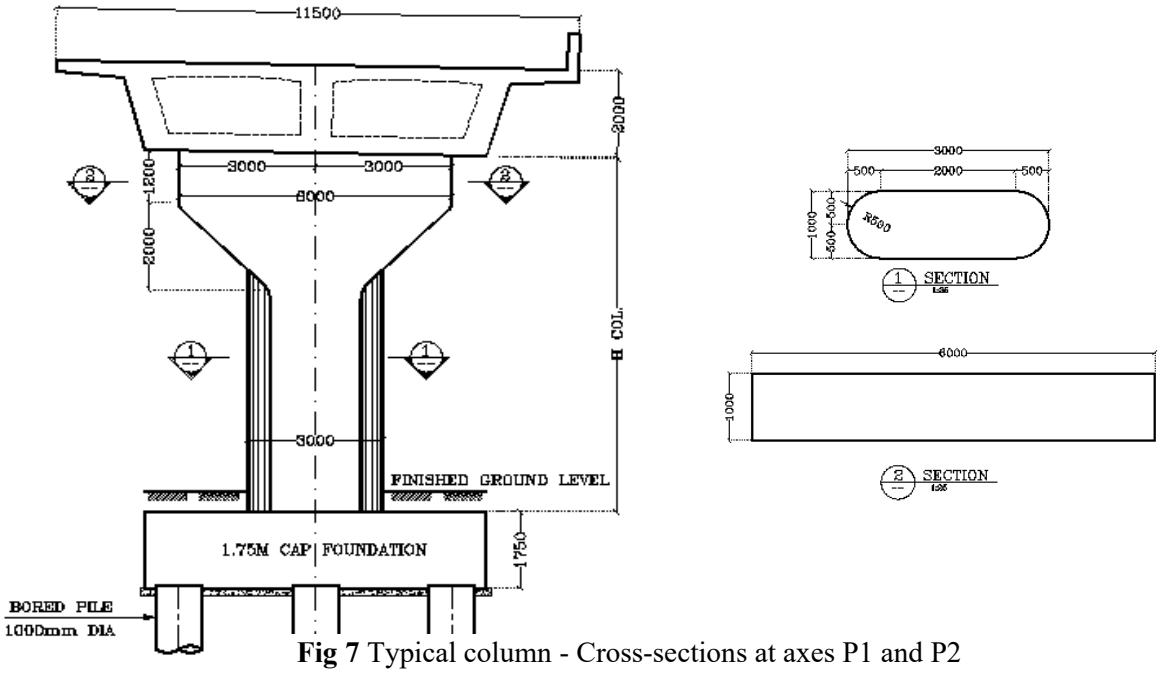

Fig 7 Typical column - Cross-sections at axes P1 and P2

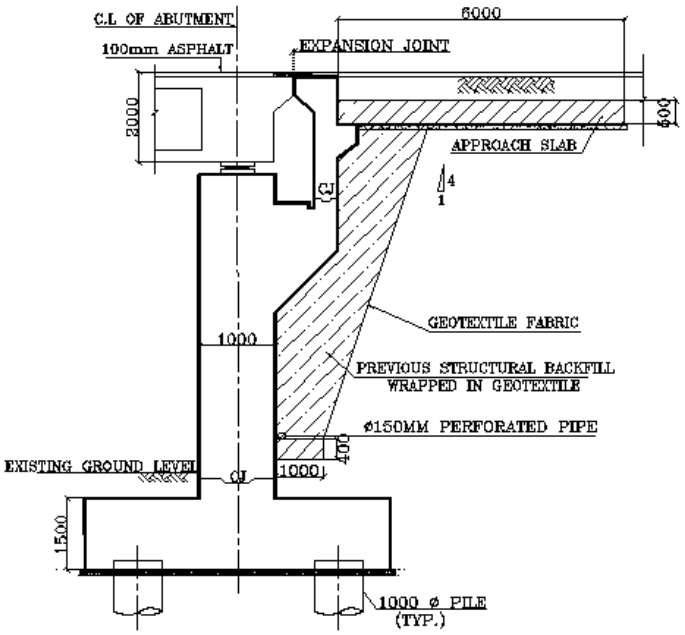

Fig 8 Typical concrete dimensions details for abutment at axes A1 and A2

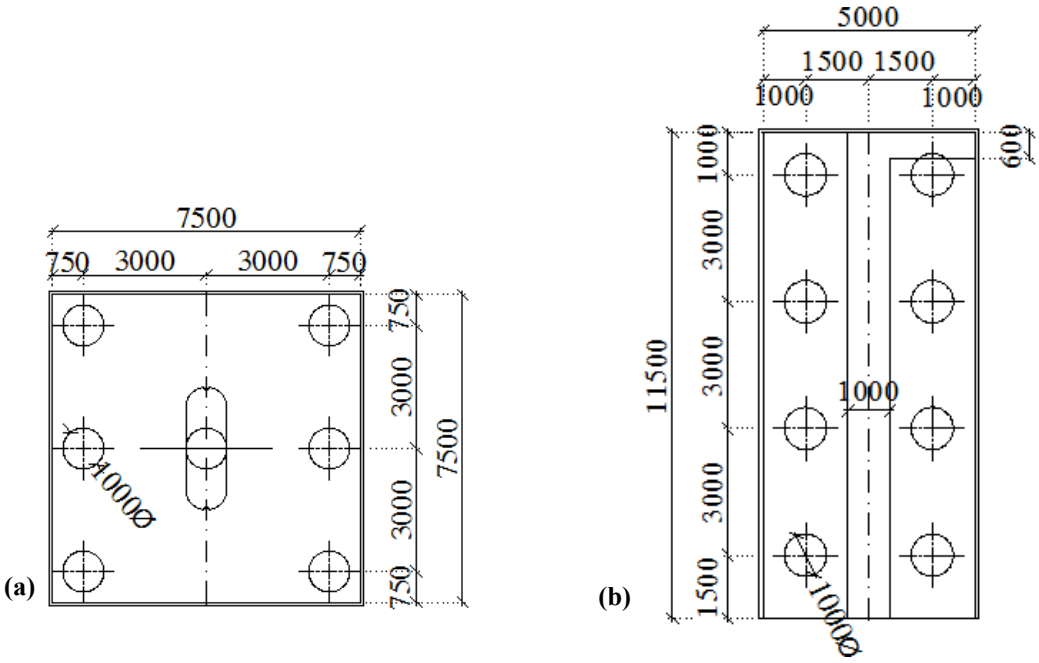

Fig 9 Boundary conditions for (a) Column foundation and (b) Abutment foundation

3.2. Bridge modeling

The grillage method was utilized to model the bridge deck. It simplifies the complex geometry of bridge models into an equivalent grid of interconnected beams or grillage members. These members represent the structural behavior of the deck, girders, and other load-carrying elements of a bridge. Section properties were calculated for each grillage element and assigned to linear elastic beam-column elements, with mass concentrated at each node in the grillage system. For the box-girder bridge, the deck section was divided into three webs, as shown in Figure 10.

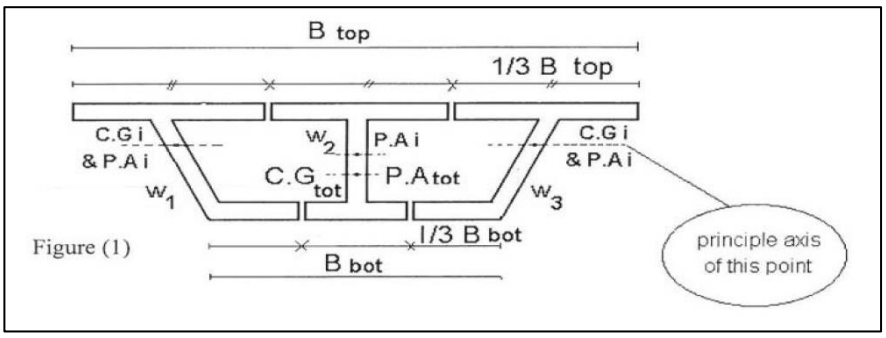

Fig 10 Grillage elements of box girders bridge

Hambly (1976) and Barker and Puckett (2007) state that the same bending and torsional stiffness parameters to grillage members as the corresponding bridge sections. Longitudinal grillage members typically align with girder centerlines, concentrating stiffness where it's most influential. Crossbeams are strategically placed to represent the deck slab. The grillage model should replicate the deflection behavior of the actual bridge deck, with similar distributions of moments, shears, and torsions in the grillage elements and the corresponding bridge sections. Figure 11 illustrates the grillage simulation of box girders bridge.

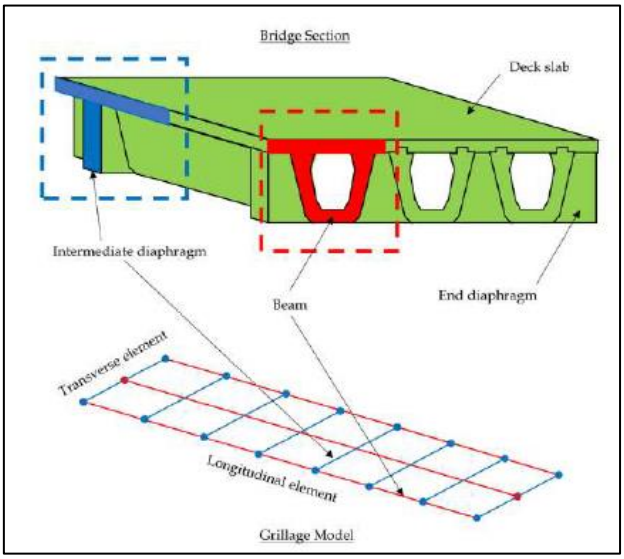

Fig 11 General grillage simulation of box girders bridge.

3.3. Developed models

In order to assess the effect of near-fault ground motions with fling-step and forward-directivity characteristics on the box girder bridge columns, six bridge models were developed and analyzed including two and three span configurations. The bridges are free for lateral movement at the edge abutments using three elastomeric bearings which represent the location of the expansion joints. The intermediate columns are connected monolithically with the bridge deck to provide the required fixation points with varying column heights from 12.0m to 9.0 m. The section properties are computed and attributed to the bridge elements within the grillage model, the deck is divided into three webs.

The employed finite elements for different elements of the box girder models are illustrated in Fig.12.

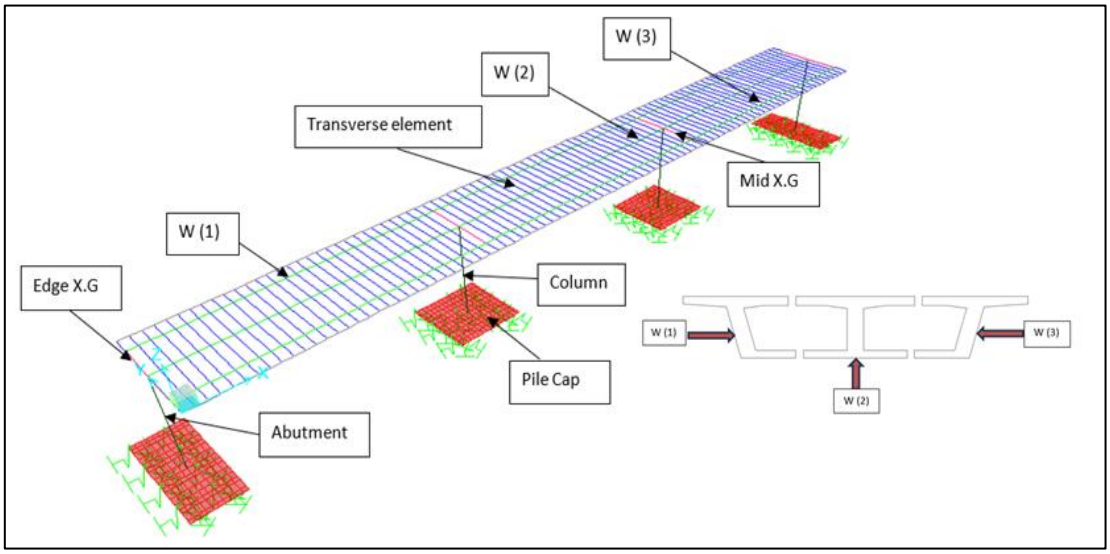

Fig 12 Grillage model of box-girder bridge

3.4. Grillage Properties of Box Girder Bridge Elements

Table 1 grillage properties of three and two spans box girder bridge

General Properties	Three and Two Spans Box Girder Bridge
Total length: Three spans / Two spans	90 / 60(m)
Span length	30(m)
Deck width	11.50(m)
Deck depth	2.0(m)
Top slab thickness	Varies from (0.30 m to 0.40 m)
Bottom slab thickness	Varies from (0.25 m to 0.40 m)
Number of piers: Three spans / Two spans	2 / 1
Dimensions of the column	Variable from (3mx1m) to (6mx1m)
Column height	Varies from 12 to 9 (m)
Number of abutments: Three spans / Two spans	2 / 2
Dimensions of the abutment	(1m depth x 11.50m width)
Abutment height	Varies from 12 to 9 (m)
Connect the deck to the abutment	3 Elastomeric Bearings
Connect the deck to the column	Monolithic
fcu (substructure)	40Mpa
fcu (Superstructure)	40Mpa
Reinforcement	360Mpa

Reference to (Hambly) the centroid of each web to be on the principal axis of the full deck section, So the deck section dived into 3 segments as shown before in figure 12. Every segment has a local axis located at its centroid, but the segment properties calculated related to the neutral axis of the full section. The properties of the employed finite elements have been assigned as the following:

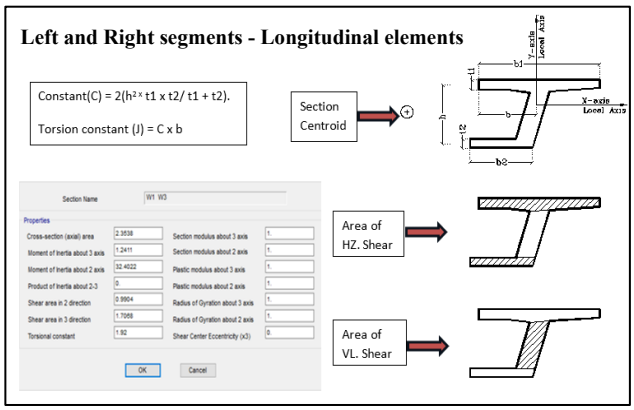

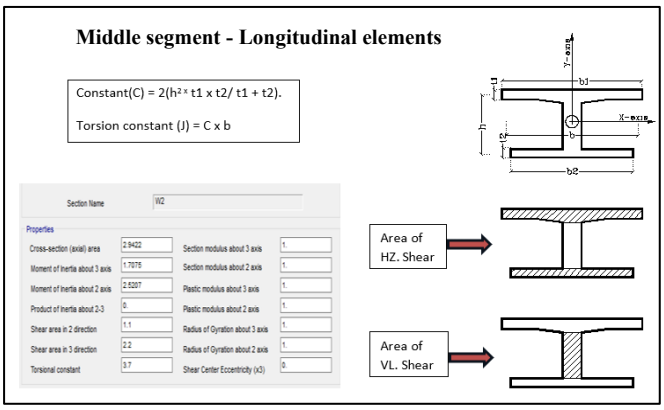

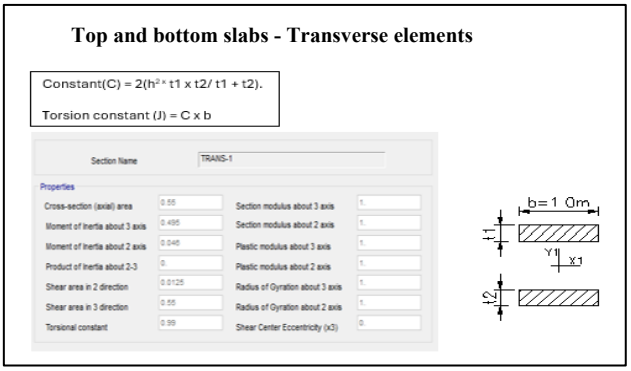

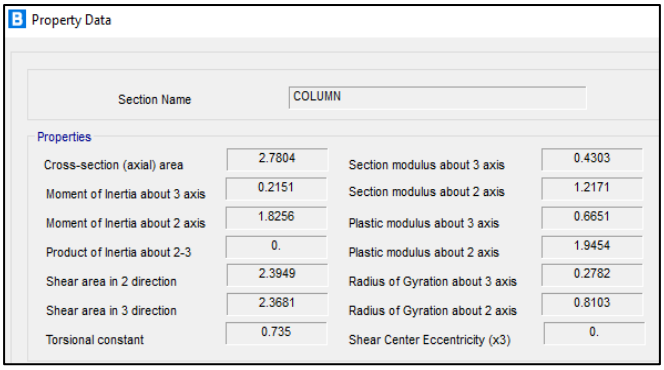

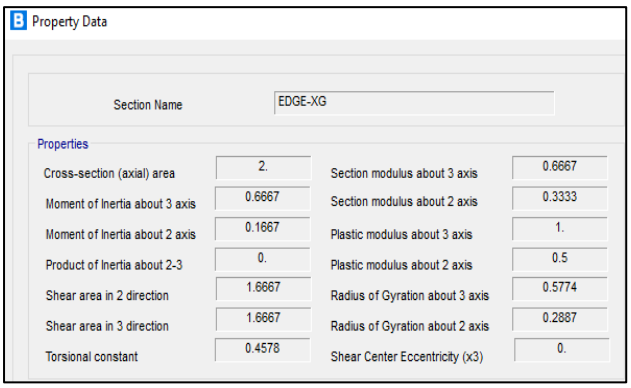

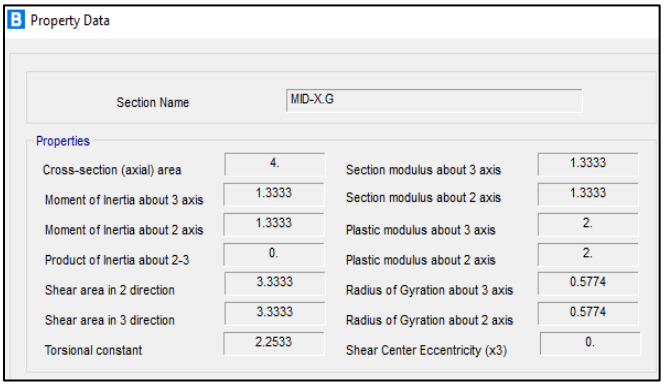

3.5. Modeling of foundation and bearing piles

The foundation boundary conditions were carefully modeled using shell finite element objects with 1.75m and 1.50m thick respectively for column and abutment pile caps to accurately represent the interaction between the bridge structure and the supporting soil, the pile caps dimensions are shown in figure 9. The soil-structure interaction (SSI) was considered by incorporating spring elements to simulate the stiffness of the supporting soil. These springs were modeled in all three translational directions (longitudinal, transverse, and vertical), with stiffness values assigned based on the

subgrade reaction modulus obtained from geotechnical investigations in the bridge location in Damanhur City as stated before in item 3.1. Soil parameters used in the modeling were derived from typical site conditions in the area. The soil profile predominantly consists of clayey silts and sandy clay layers with varying degrees of stiffness. the pile capacity is 2700 kN with 20m deep and approximate settlement of 10mm.the pile working as end bearing pile with a vertical stiffness of 270000 kN/m while the lateral stiffness is 30000 kN/m. Foundation models are shown in figure 13.

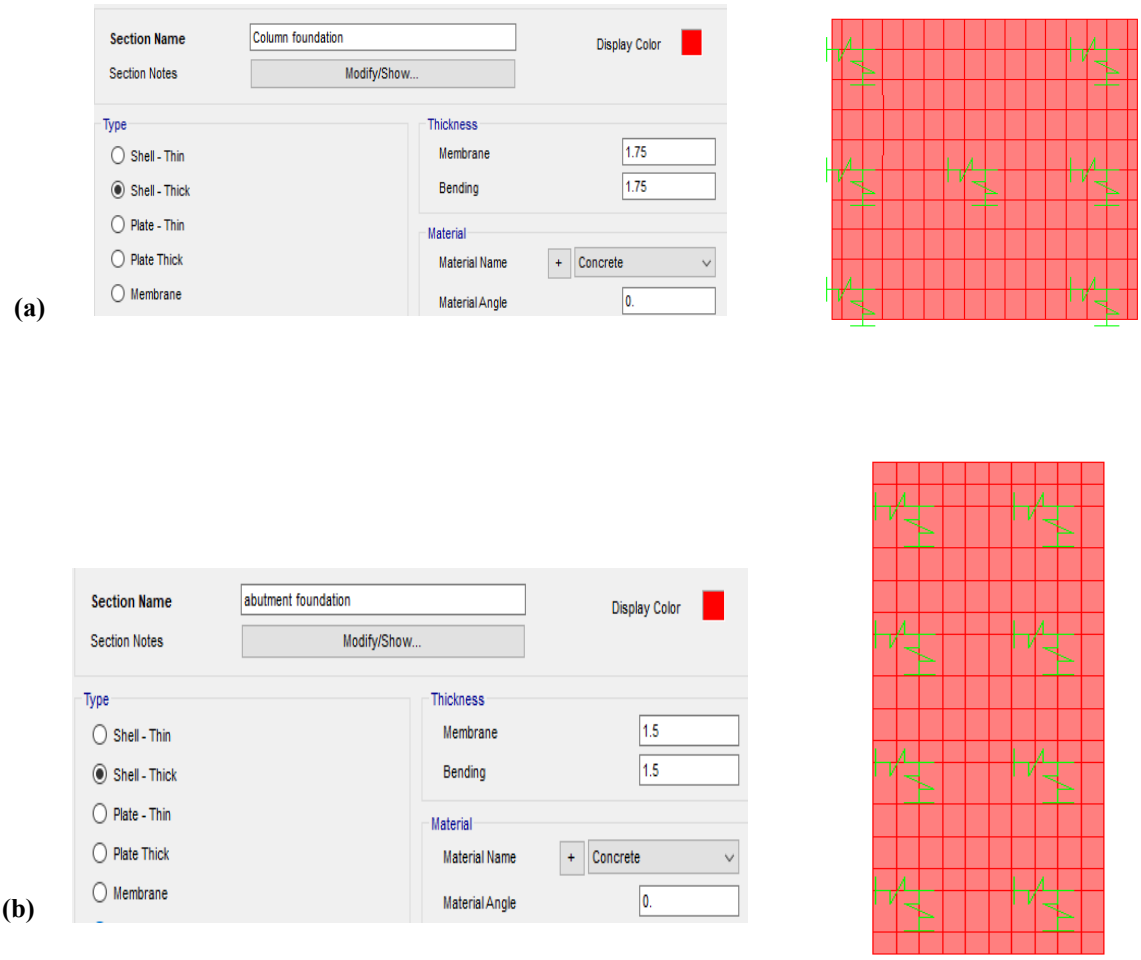

Fig 13 Modeling for (a) Columns pile cap and (b) Abutments pile cap

3.6. Verifications of the grillage method

To ensure the reliability and accuracy of the grillage model, Comparison with 3D Finite Element Models (FEM) of the box girder bridge, incorporating shell elements to accurately capture the behavior of the deck, webs, flanges, diaphragms, and torsional effects have been carried out.

The dead load deformation obtained from the grillage method demonstrated 98.2% accuracy compared to the 3D Finite Element Model (FEM) results. The grillage model predicted a total deadload deflection of 16.8 mm as shown in figure 14, whereas the FEM model gave 17.1 mm as shown in the corresponding 3D FEM model, figure 15.

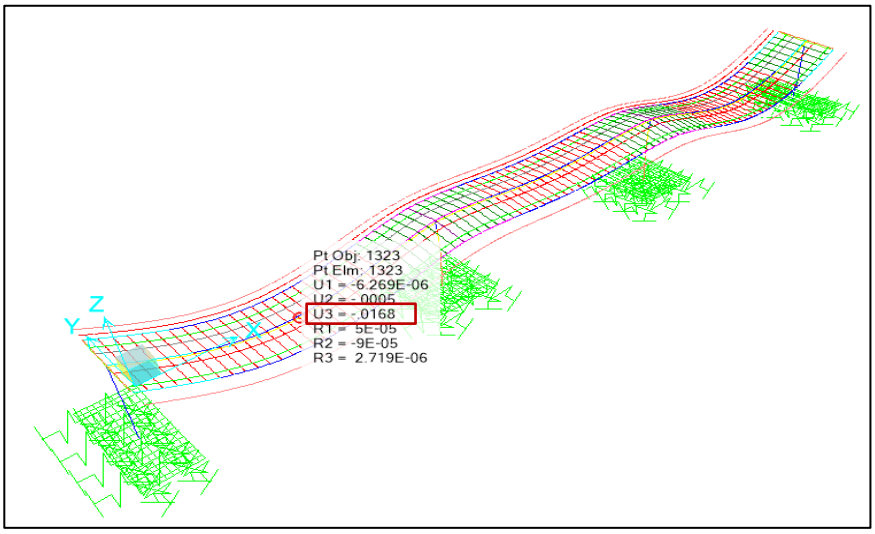

Figure 14 Grillage model of box girders bridge.

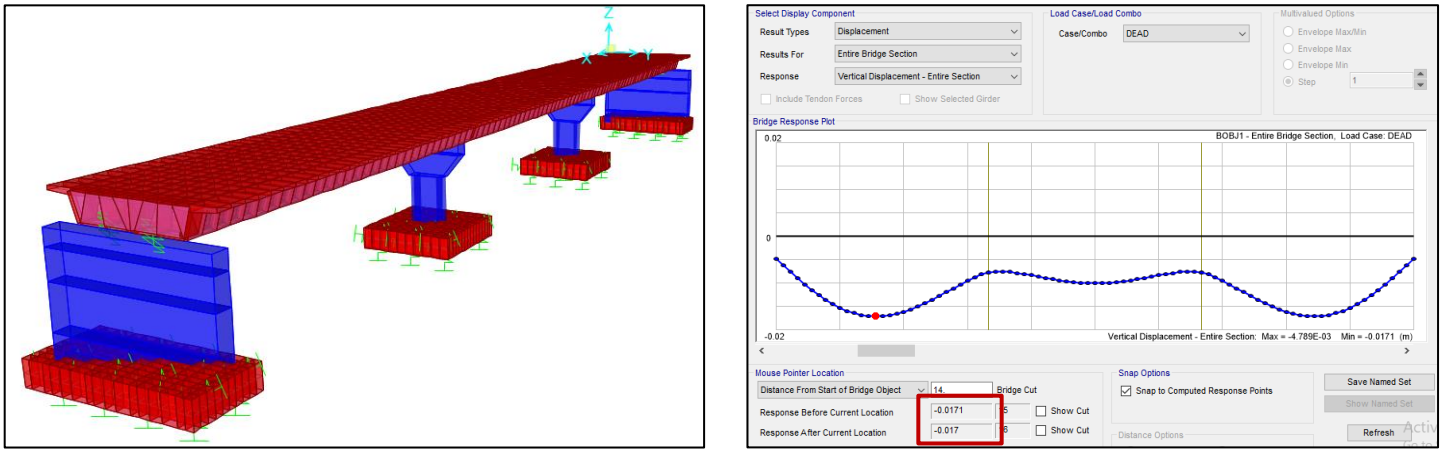

Fig 15 3D FEM model of box girders bridge

4. Utilized Ground Motion Records

Fling step and forward directivity are two distinct effects observed in ground motion during large earthquakes, primarily near fault zones. Both are related to the rupture process of the fault, but they have different physical causes and manifestations as the following:

4.1. Fling Step

Results from permanent tectonic deformation as the fault slips and the ground shifts permanently to a new position. often termed a "reversing form," as illustrated in the Chi-Chi-EW TCU068 velocity time history as shown in Fig. 16

Characteristics:

- Produces a long-period, one-sided pulse in the velocity time history, meaning the ground moves in one direction and stays displaced.

4.2. Forward-directivity

Occurs when the fault rupture propagates toward a site at a velocity close to the shear wave speed, concentrating seismic energy in the direction of rupture. It features a two-sided pulse, or "non-reversing form," as exemplified by the Loma-Prieta from the LGPC station velocity time-history as shown in Fig. 16. This pulse type did not perform any permanent ground displacement

Characteristics:

- Produces a high-amplitude, short-duration pulse in the velocity time history, often referred to as a "pulse-like" ground motion

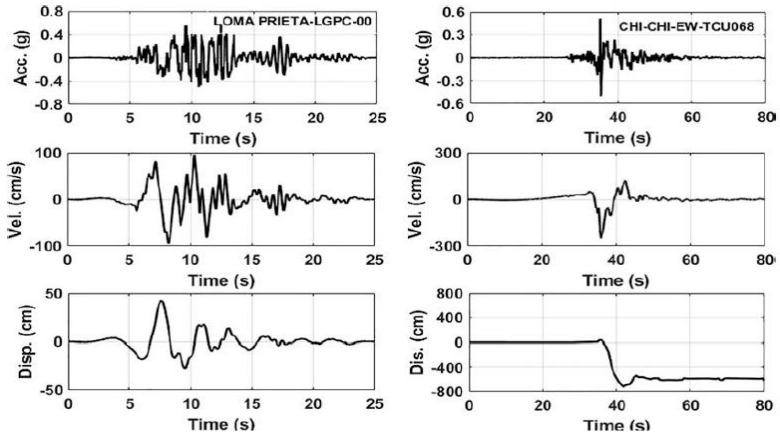

Fig 16 Acceleration, velocity, and displacement time-histories of Loma Prieta-LGPC and Chi-Chi-TCU068 as representatives of forward directivity and fling-step records, respectively

Fourteen near-fault earthquake records, categorized into forward-directivity and fling-step events, have been considered during the study. Table 2 provides the dataset sourced from the Pacific Earthquake Engineering Research Center (PEER).To align with Cairo city conditions, all records were scaled to a PGA of 0.125g.

Table 2. Utilized ground motion records with forward directivity and fling step characteristics

Earthquake (record)	Station	Type	PGA (g)	PGV (cm/sec)	PGD (cm)	PGA/ PGV	M_w	t_d (s)
Cape-Mendocino	Petrolia-90	FD	0.66	88.5	33.2	0.75	7.0	25
Erzincan-EW	Pacoima Dam 279	FD	0.50	78.12	28.02	0.64	6.7	20
Tabas	Ferdows	FD	0.87	123.3	93.57	0.71	7.3	32
Loma-Prieta	LGPC-00	FD	0.57	96.05	41.92	0.59	6.9	25
Loma-Prieta	Lexdam-00	FD	0.41	95.73	30.27	0.43	6.9	15
Northridge	Rinaldi-228	FD	0.87	147.92	41.86	0.59	6.7	15
Northridge	Oliveview-360	FD	0.84	129.31	32.11	0.65	6.7	15
Chi-Chi NS	TCU-052	FS	0.45	172.24	226.5	0.26	7.6	90
Chi-Chi EW	TCU-052	FS	0.36	151.13	210.3	0.24	7.6	90

Chi-Chi EW	TCU-065	FS	0.79	125.28	108.7	0.63	7.6	90
Chi-Chi EW	TCU-068	FS	0.51	248.50	297.0	0.21	7.6	90
Chi-Chi NS	TCU-068	FS	0.37	263.96	421.0	0.14	7.6	90
Chi-Chi EW	TCU-074	FS	0.59	70.33	21.31	0.84	7.6	90
Chi-Chi NS	TCU-084	FS	0.43	48.07	20.44	0.89	7.6	90

5. Results

5.1. Bridge Modelling Groups

The bridge models have been divided into two groups as shown below.

Table 3. Characteristics of Group No.1.

Model No.	No of span	Span length(m)	Column height (m)	Deck cross section
1	3	30-30-30	12.0	Box Girder
2	3	30-30-30	10.5	Box Girder
3	3	30-30-30	9.0	Box Girder

Table 4. Characteristics of Group No. 2.

Model No.	No of span	Span length(m)	Column height (m)	Deck cross section
4	2	30-30	12.0	Box Girder
5	2	30-30	10.5	Box Girder
6	2	30-30	9.0	Box Girder

5.2. Results of Group No.1- Longitudinal direction

This group illustrates the outcomes of the finite element models for box-girder bridges, each with three spans of 30m, two intermediate columns with column heights vary from 12.0m to 9.0m in addition to two edge abutments.

5.2.1. Columns Displacement Response

It is observed that the column horizontal displacement responses obtained along its variable height for the considered different bridge models, in terms of box-girder, under the excitation of forward-directivity and fling-step records are presented in a comparative way in figure 17, The figures were

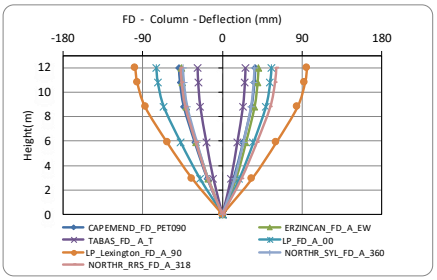

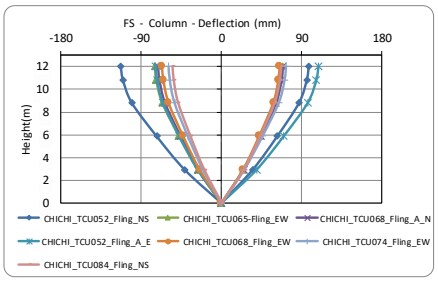

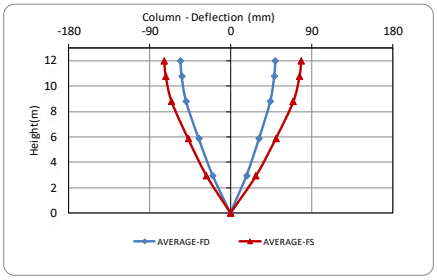

arranged according to the column's height in descending order of height to facilitate a comparison of performance between different outcomes.

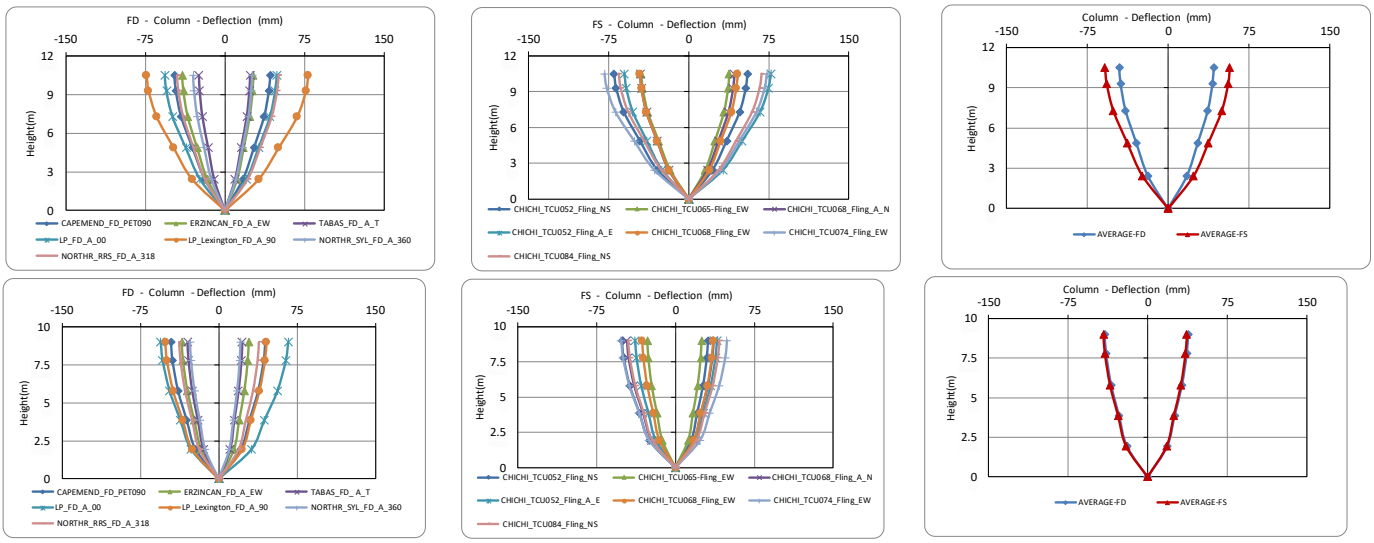

Fig 17 Column's peak displacements and average of peaks against column's heights varying from 12m to 9m obtained under forward directivity and fling-step records for box-girder bridges

The displacement responses reach peak values at the top of the column height across all the bridge models and earthquake records considered. The average peak displacements recorded at the top of the column under fling-step records are 78.32mm, 58.64mm and 41.58mm for column heights of 12m, 10.5m, 9m respectively. The corresponding values under the forward directivity records are respectively 50.08mm, 45.30mm and 40.50mm. the plotted mean values clearly indicate that the records with fling-step produce higher average displacement values compared with those obtained under the forward-directivity records for the considered bridge models by about 56%, 29 % and 3 % for models with column heights of 12m, 10.5m and 9m respectively.

5.2.2. Columns Rotation Response

The column's rotation response obtained along the column's height for all considered different bridge models under the excitation of forward-directivity and fling-step are presented in figure18

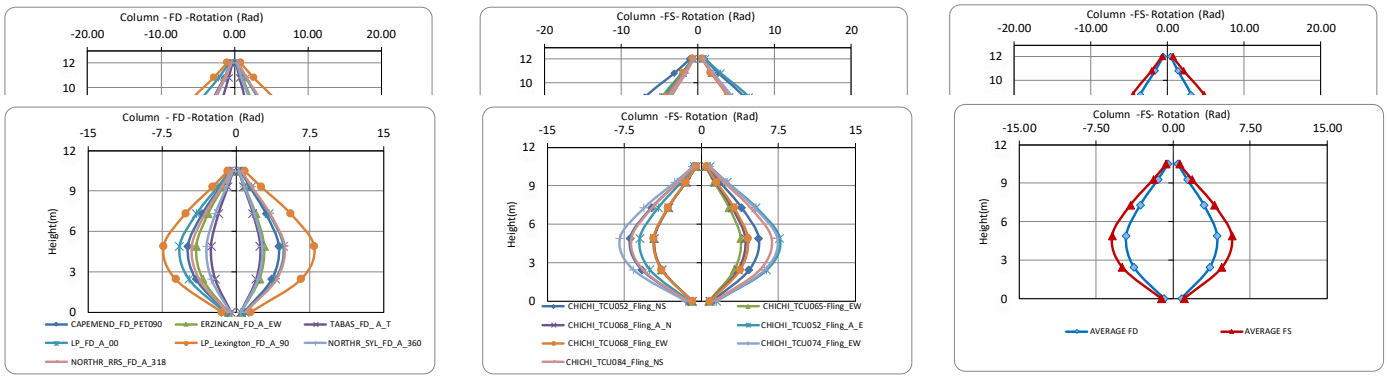

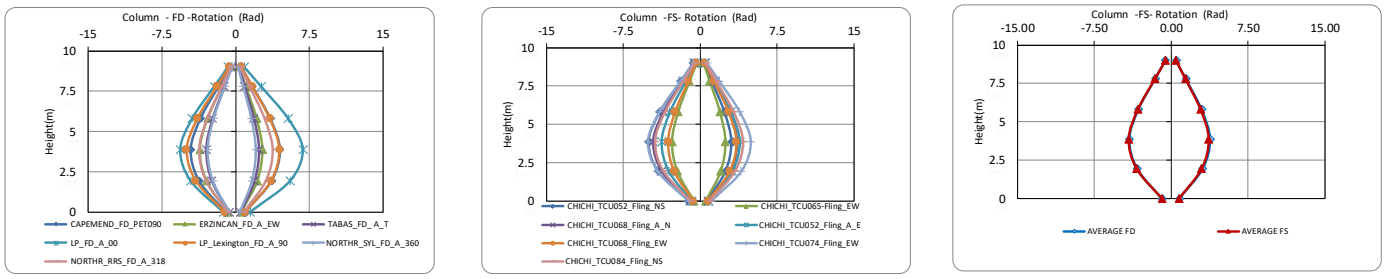

Fig 18 Column's peak rotation and average of peaks against column's heights varying from 12m to 9m obtained under forward directivity and fling-step records for box-girder bridges

The rotation response curves closely follow a sinusoidal shape, with the peak rotation occurring near the first quarter of the column height from the base. The average peak rotation values recorded due to fling-step events are 7.62 rad, 5.73 rad and 4.11 for column heights of 12m, 10.5m, 9m respectively. The corresponding values under the forward directivity records are respectively 4.92rad, 4.30 rad and 4.05 rad. These values show an increase in the rotational demand of about 53%, 33 % and 1 % for models with column heights of 12m, 10.5m and 9m respectively.

5.2.3. Columns Bending Moment Response

The column's bending moment response obtained along its height for all considered different bridge models under the excitation of forward-directivity and fling-step are presented in figure19

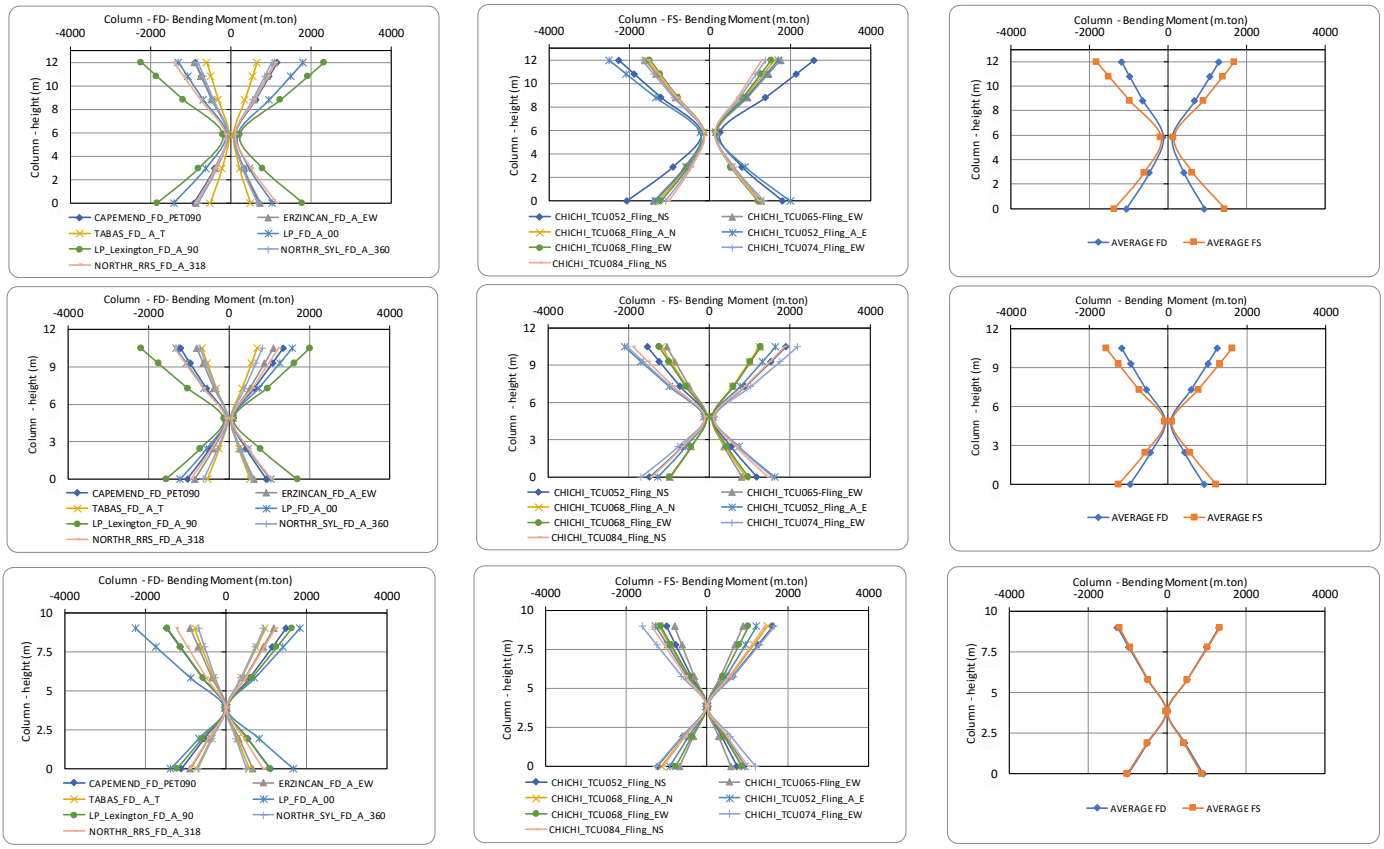

Fig 19 Column's peak bending moment and average of peaks against column's heights varying from 12m to 9m obtained under forward directivity and fling-step records for box-girder bridges

The highest moment values are observed at both the top and bottom of the column, regardless of the type of applied records. Analyzing the moment distribution along the column height reveals that the lowest moment value is concentrated around the middle of the column. The average peak bending moment recorded at the bottom of the column under fling-step records are 1445, 1219 and 1001m.ton for box-girder models with column heights of 12m, 10.5m and 9m respectively. While at top of the column are 1811, 1574 and 1340m.ton corresponding values under the forward directivity records at bottom section are respectively 931, 914 and 985m.ton. While at the top section are 1171, 1181 and 1321m.ton. The plotted mean values clearly indicate that the records with fling-step produce higher average bending moment values compared with those obtained under the forward-directivity records for all the considered bridge models by about 55% ,33% and 1.50% for models with column heights of 12m, 10.5m and 9m respectively.

5.2.4. Columns Shear Force Response

The column shear force responses obtained along its variable height for the considered different bridge models under the excitation of forward-directivity and fling-step records are presented in figure 20

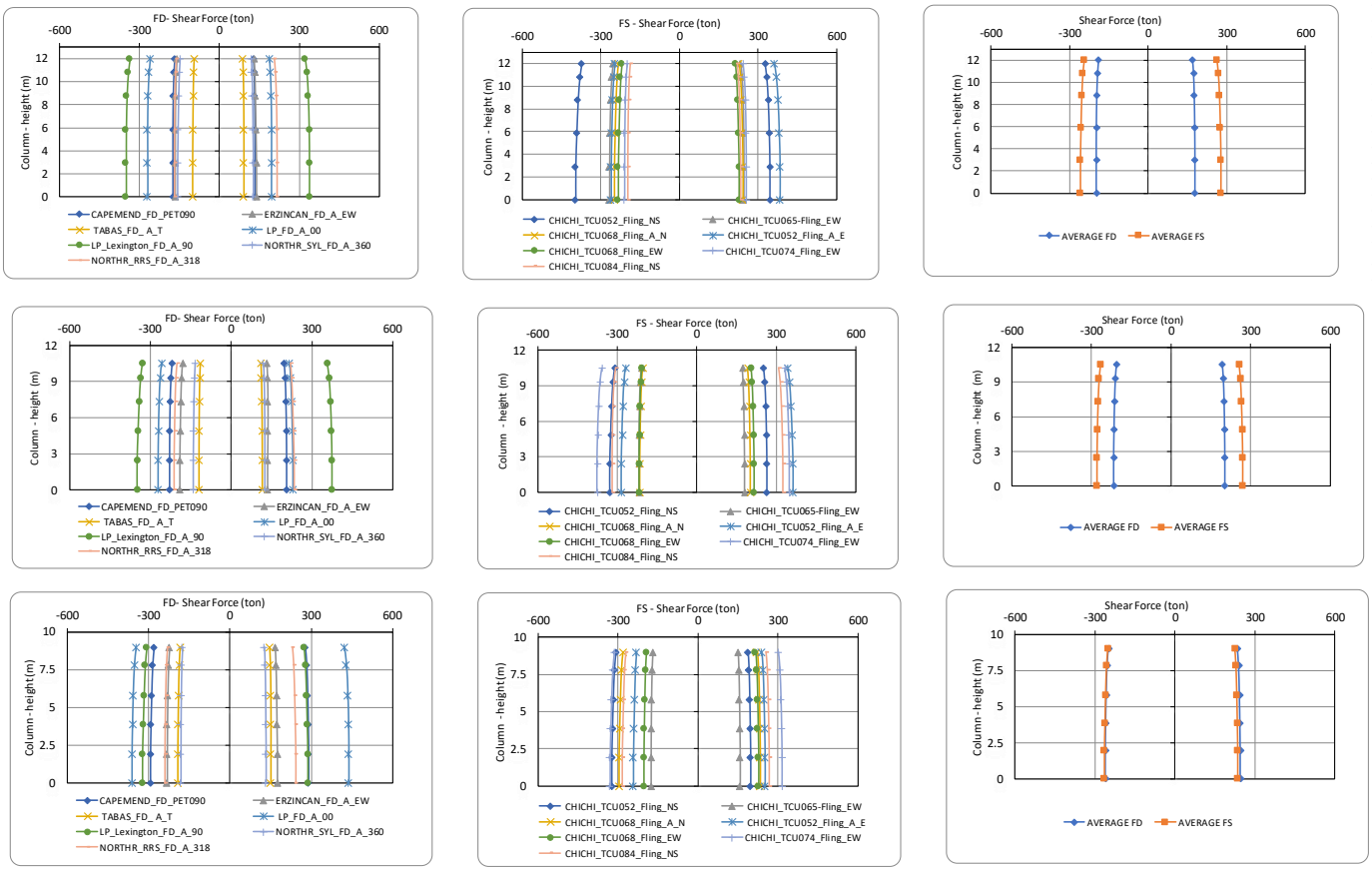

Fig 20 Column's peak shear force and average of peaks against column's heights varying from 12m to 9m obtained under forward directivity and fling-step records for box-girder bridges

The shear forces observed nearly constant along the column height across all bridge models and earthquake records considered. The average peak shear force values recorded under fling-step events are 276, 280 and 265ton for box-girder models with column heights of 12m, 10.5m and 9m respectively. The corresponding values under the forward directivity records are respectively 178, 215 and 260ton. These values show an increase in the shear force demand of about 55%, 30% and 1 % for models with column heights of 12m, 10.5m and 9m respectively.

Results of Group No.2- Longitudinal direction

This group illustrates the outcomes of the finite element models for box-girder bridges, each with two spans of 30m, one intermediate column with column heights varies from 12.0 to 9.0 m in addition to two edge abutments.

5.2.5. Columns Displacement Response

The column horizontal displacement responses obtained along with its variable height for the different bridge models, in terms of box-girder, under the excitation of forward-directivity and fling-step records are presented in a comparative way in figure 21 in descending order of height.

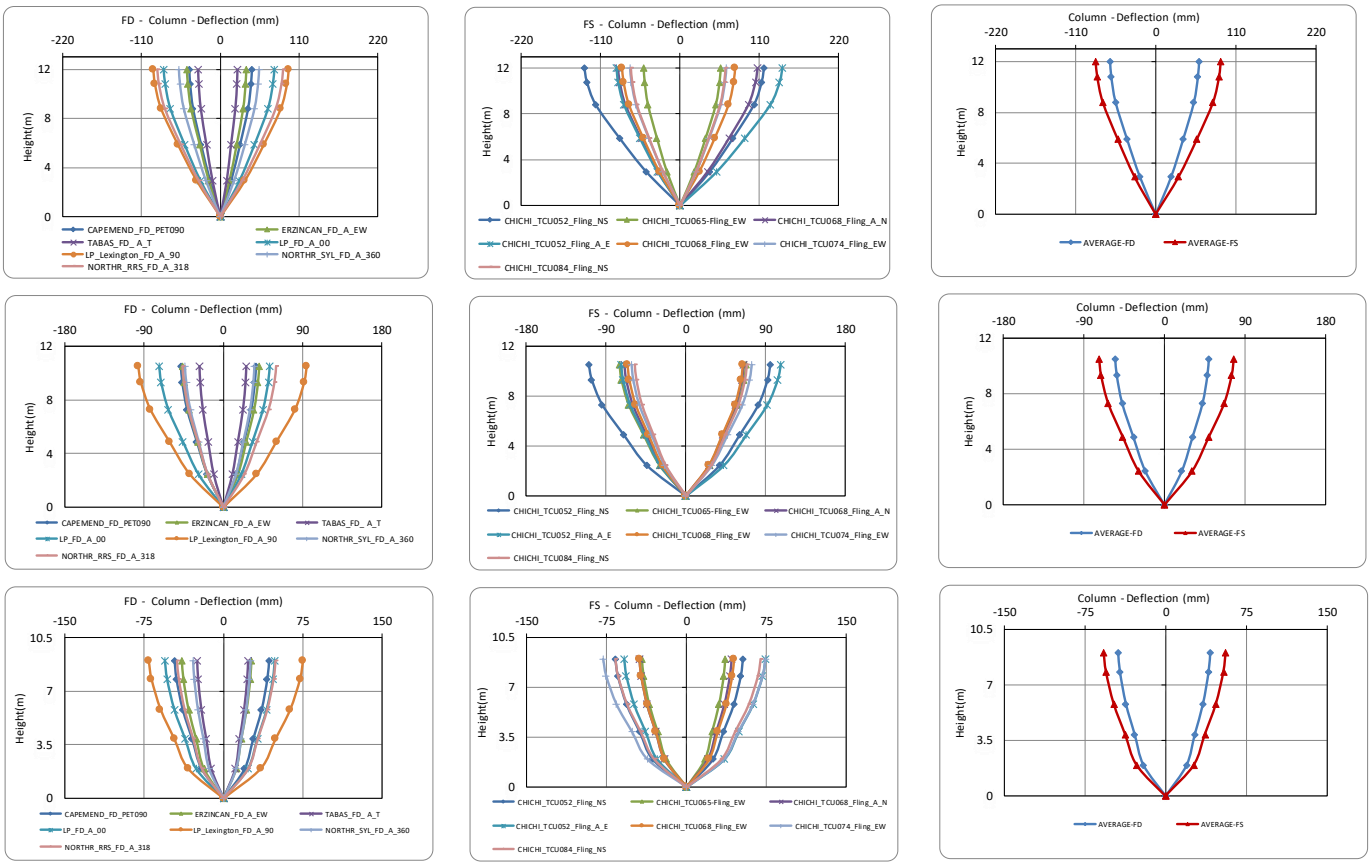

Fig 21 Column's peak displacements and average of peaks against column's heights varying from 12m to 9m obtained under forward directivity and fling-step records for box-girder bridges

It is observed that the displacement responses generally reach peak displacement at the top of the column height across all the bridge models and earthquake records considered. The average peak displacements recorded at the top of the column under fling-step records are 89.35mm, 77.36mm and 56mm for column heights of 12m, 10.5m and 9m respectively. The corresponding values under the forward directivity records are respectively 59.38mm, 49.36mm and 41.42mm. The plotted mean values clearly indicate that the records with fling-step produce higher average deflection values compared with those obtained under the forward-directivity records for the considered bridge models by about 50%, 57% and 35% for column heights of 12m, 10.5m and 9m respectively.

5.2.6. Columns Rotation Response

The column's rotation response obtained along with the column's height for all considered different bridge models under the excitation of forward-directivity and fling-step are presented in figure 22

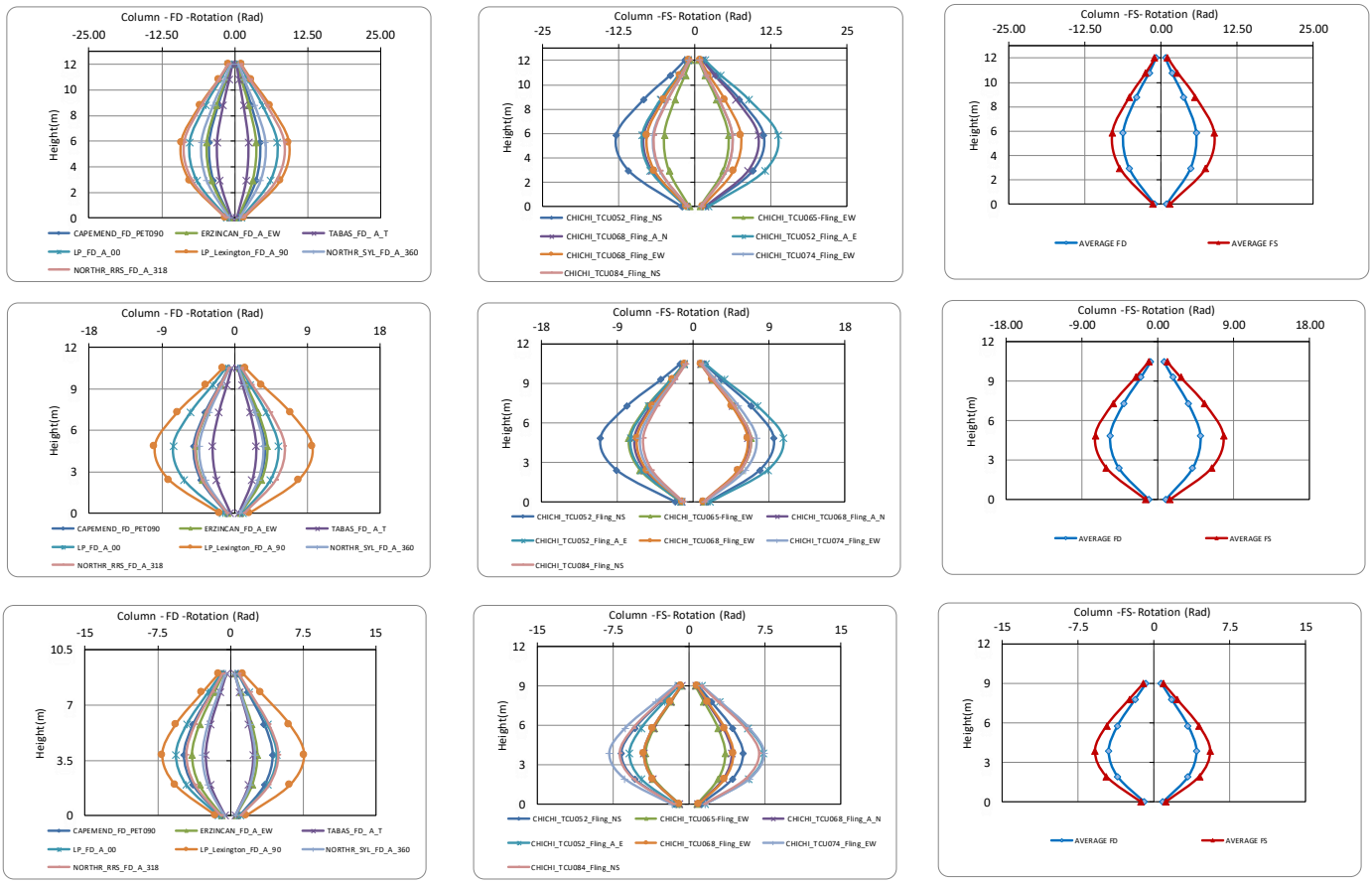

Fig 22 Column's peak rotation and average of peaks against column's heights varying from 12m to 9m obtained under forward directivity and fling-step records for box-girder bridges

The rotation responses of the column exhibit similar patterns to those observed in longitudinal displacement. However, the rotation response curves closely follow a sinusoidal shape, with the peak rotation occurring near the first quarter of the column height from the base. The average peak rotation values recorded due to fling-step events are 8.71, 7.80 rad and 5.60 rad for box-girder models with

column heights of 12m, 10.5m and 9m respectively. The corresponding values under the forward directivity records are respectively 5.83rad, 5.04rad and 4.19rad. These values show an increase in the rotational demand of about 49%, 55% and 34% for models with column heights of 12m, 10.5m and 9m respectively.

5.2.7. Columns Bending Moment Response

The column's bending moment response obtained along its height for all considered different bridge models under the excitation of forward-directivity and fling-step are presented in figure23.

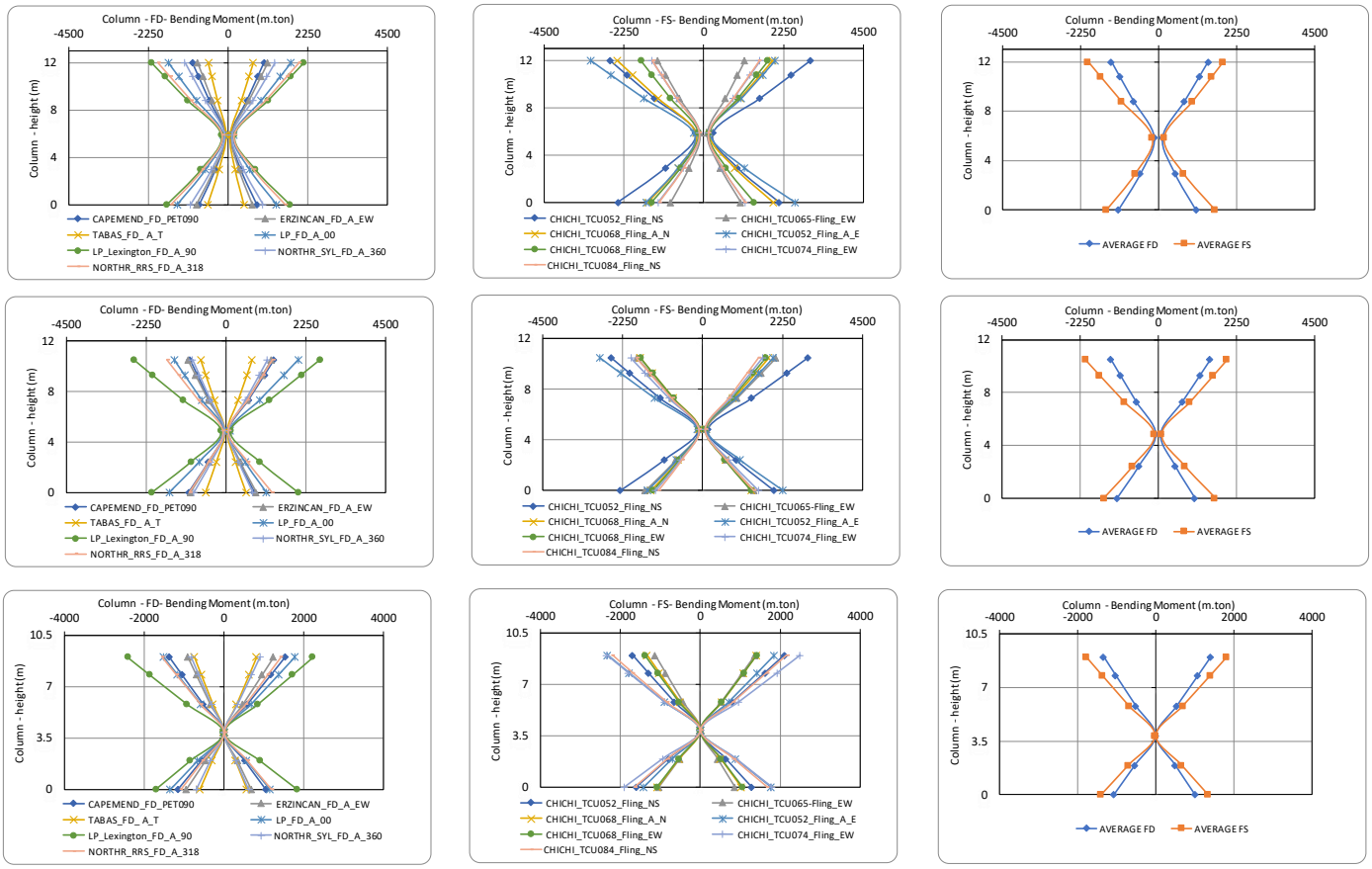

Fig 23 Column's peak bending moment and average of peaks against column's heights varying from 12m to 9m obtained under forward directivity and fling-step records for box-girder bridges

As shown in the figure, the highest moment values are observed at both the top and bottom of the column, regardless of the type of applied records. Analyzing the moment distribution along the column height reveals that the lowest moment value is concentrated around the middle of the column. The average peak bending moment recorded at the bottom of the column under fling-step records are 1634, 1642 and 1348m.ton for column heights of 12m, 10.5m and 9mrespectively. While at top of the column are 2026, 2091 and 1771m.ton corresponding values under the forward directivity records at bottom section are respectively 1091, 1060 and 1009m.ton. While at the top section are 1355, 1353 and 1329. From percentage point of view, the plotted mean values clearly indicate that the records with fling-step

produce higher average bending moment values compared with those obtained under the forward-directivity records for all the considered bridge models by about 53% ,55% and 33.50% for models with column heights of 12m, 10.5m and 9m respectively.

5.2.8. Columns Shear Force Response

The column shear force responses obtained along its variable height for the considered different bridge models, under the excitation of forward-directivity and fling-step records are presented in figure 24.

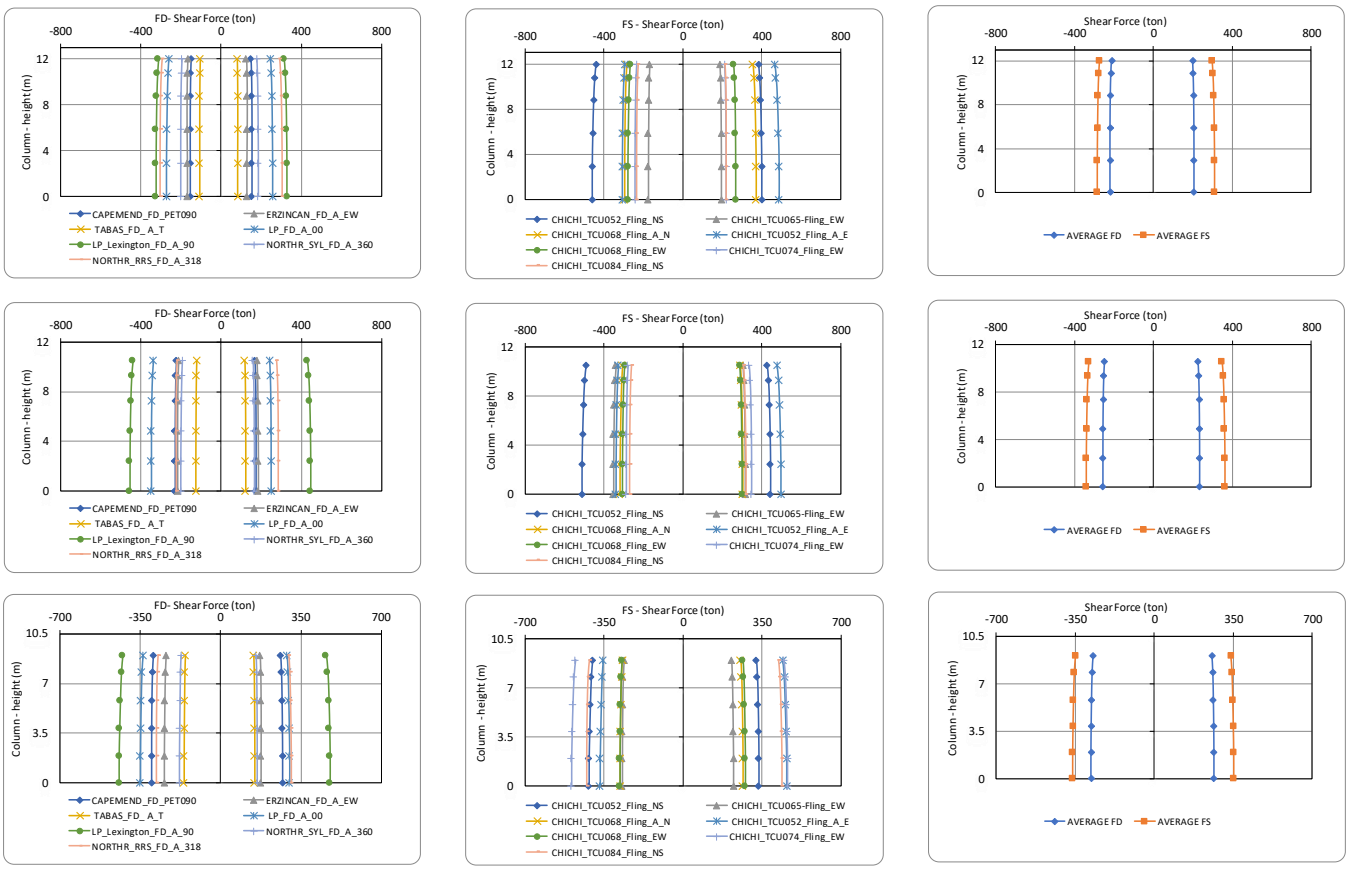

Fig 24 Column's peak shear force and average of peaks against column's heights varying from 12m to 9m obtained under forward directivity and fling-step records for box-girder bridges

The shear forces observed nearly constant along the column height across all bridge models and earthquake records considered. The average peak shear force values recorded under fling-step events are 309, 346 and 351 ton for box-girder models with column heights of 12m, 10.5m and 9m respectively. The corresponding values under the forward directivity records are respectively 206, 224 and 263 tons. These values show an increase in the shear force demand of about 50%, 54%, and 33% for models with column heights of 12m, 10.5m and 9m respectively.

6. Results Analysis

6.1. Span to column height (L/H) effect on fling-step and forward directivity response

The developed models are categorized into two groups with different column heights ranging from 12 m to 9 m. The study demonstrates that the seismic responses to forward-directivity ground motions differ significantly from those caused by fling-step ground motions. For models with three and two spans, the average longitudinal straining action values are consistently higher for fling-step records compared to forward-directivity records across all bridge models with column heights of 12 m, 10.5 m, and 9 m, corresponding to L/H ratios of 2.50, 2.85, and 3.33, respectively. The following charts illustrate the percentage difference in the longitudinal output responses between fling-step and forward-directivity records for columns straining actions.

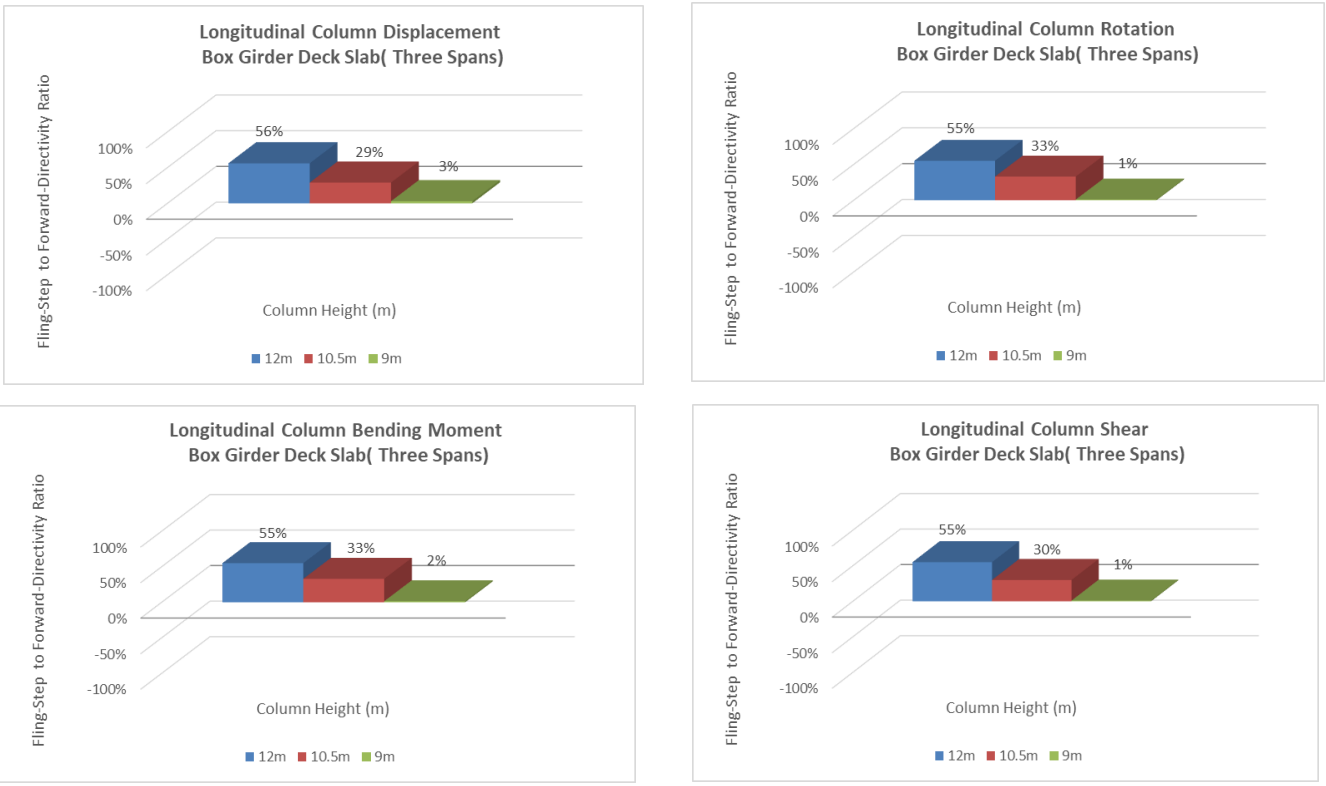

Fig 25 The percentage difference between fling step and forward directivity effects in the longitudinal straining actions of columns for three spans bridge models considering the variations in column height

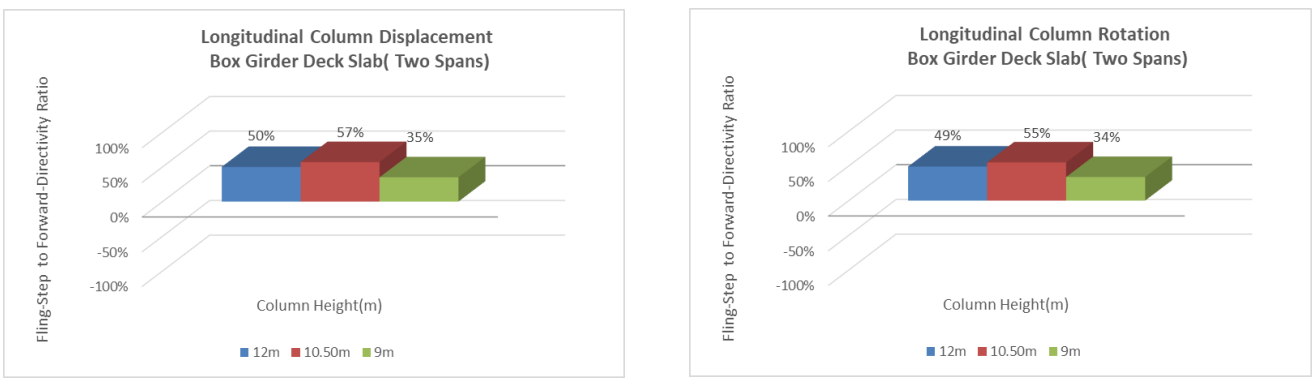

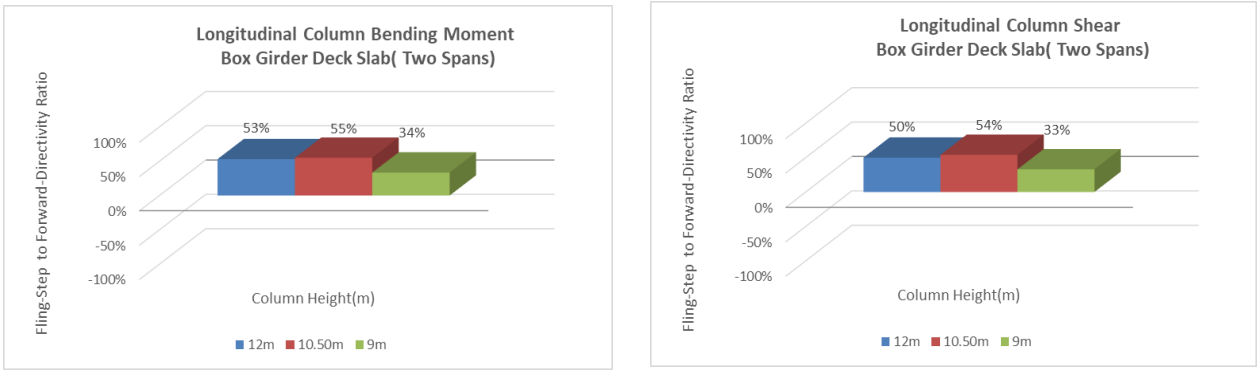

Fig 26 The percentage difference between fling step and forward directivity effects in the longitudinal straining actions of columns for two spans bridge models considering the variations in column height

6.2. Number of spans influence on the fling-step and forward directivity responses

The comparison of column responses for bridges with varying numbers of spans shows that the performance differs regarding the forward-directivity and fling-step effects. Two-span models generally show higher straining actions than three-span models. Furthermore, the straining actions in two-span bridges are more intense under fling-step effects than in three-span bridges. This result leads to a larger disparity between responses of fling-step to forward-directivity effects compared to three-span models which reveals that the number of spans has a significant impact on the bridge design strategy. The following charts demonstrate how altering the number of spans from three to two affects the longitudinal responses of columns under fling-step and forward-directivity records along with the straining actions across the analyzed groups.

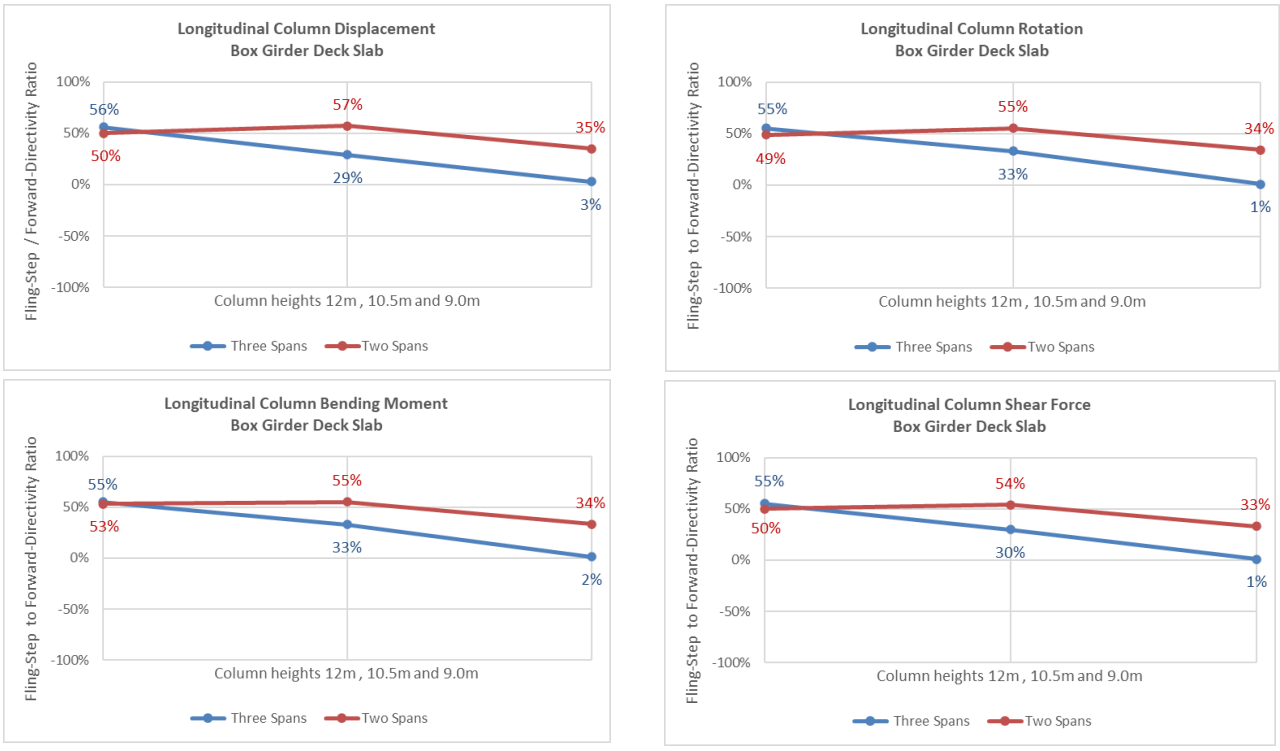

Fig 27 Number of spans influence on the percentage difference between fling-step and forward directivity responses in the longitudinal straining actions of columns considering the variations in column height

7. Conclusions

This study investigates the effects of forward-directivity and fling-step ground motions on the seismic performance of reinforced concrete (RC) box girder bridges. Bridge models with box sections were developed and subjected to fourteen ground motion records representing both forward-directivity and fling-step characteristics. All models share identical span lengths and deck widths. The seismic responses were evaluated through nonlinear analysis, leading to the following conclusions based on the simulation results:

1- The study reveals that the seismic responses of box girder bridge columns to forward-directivity ground motions differ significantly from those induced by fling-step ground motions. The mean response values indicate that the average straining actions associated with fling-step records are consistently approximately 55% higher than those resulting from forward-directivity records across all evaluated parameters. This disparity is most significant in taller columns and gradually decreases as column height is reduced.

2- For the bridge models subjected to forward-directivity ground motions, the column responses increase with a higher PGV/PGA ratio. Among these records, the Loma Prieta earthquake, which exhibits the highest PGV/PGA ratio, produces the greatest response values.

3- Among the bridge models subjected to fling-step ground motions, the Chi-Chi earthquake records from station TCU-052 generate the highest straining action values compared to the other records, particularly those from station TCU-084. This difference may be attributed to the presence of distinct pulses in both the acceleration and velocity time histories of the TCU-052 records.

4- Two-span bridge models generally exhibit higher straining actions than their three-span models. Moreover, the straining actions in two-span bridges are more pronounced under fling-step ground motions compared to those observed in three-span bridges.

5- Reducing the number of spans from three to two significantly amplifies the difference in seismic response between fling-step and forward-directivity ground motions. As shown in Figure 27, fling-step records result in approximately 57% greater displacements than forward-directivity records in two-span models, compared to a 29% difference in three-span models with a column height of 10.50 m. For columns with a height of 9 m, the displacement difference reaches 35% in two-span models, while it decreases to just 3% in three-span models.

References

[1] Near-fault Ground Motions for Seismic Design of Bridge Structures, Wu, Shuanglan, Kyoto University, 2018-03-26 . https://doi.org/10.14989/doctor.k21084.

[2] Kawashima K. Damage of bridges resulting from fault rupture in the 1999 Kocaeli and Duzce, Turkey earthquakes and the 1999 Chi-Chi, Taiwan earthquake. Struct Eng/Earthquake Eng 2002;19(2):179.

[3] Bray JD, Rodriguez-Marek A. Characterization of forward-directivity ground motions in the near-fault region. Soil Dyn Earthquake Eng 2004;24(11):815–828. http://dx.doi.org/10.1016/j.soildyn.2004.05.001

[4] Makris N, Black CJ. Evaluation of peak ground velocity as a "good" intensity measure for near-source ground motions. J Eng Mech 2004;130(9):1032–1044. https://doi.org/10.1061/(ASCE)0733-9399(2004)130:9(1032)

[5] Adanur, S., Altunişik, A.C., Bayraktar, A. et al. Comparison of near-fault and far-fault ground motion effects on geometrically nonlinear earthquake behavior of suspension bridges. Nat Hazards 64, 593–614 (2012). https://doi.org/10.1007/s11069-012-0259-5

[6] Yadav KK, Gupta VK. Near-fault fling-step ground motions: characteristics and simulation. Soil Dyn Earthq Eng 2017;101:90–104. https://doi.org/10.1016/j.soildyn.2017.06.022

[7] Liao, WI., CH. Loh, and BH. Lee, "Comparison of Dynamic Response of Isolated and Non-Isolated Continuous Girder Bridges Subjected to Near-Fault Ground Motions", Engineering Structures, Vol. 26, pp. 2173-2183, July 2004.

[8] Chen X, Xiang NL, Li JZ, Guan ZG. Influence of near-fault pulse-like motion characteristics on seismic performance of tall pier bridges with fragility analysis. J Earthq Eng 2022; 26(4): 2001-2022. https://doi.org/10.1080/13632469.2020.1751345

[9] Li J, Xu LH. Seismic response characteristics and whiplash effect mechanism of continuous rigid-frame bridges subjected to near-fault ground motions. Bull Earthq Eng 2023; 21: 3719-3744. https://doi.org/10.1007/s10518-023-01672-4

[10] Mahmoud S, Alqarni A, Saliba J, H. Ibrahim A, Genidy M, Diab H. Influence of floor system on seismic behavior of RC buildings to forward directivity and fling-step in the near-fault region. Structures 2021; 30:2 803-817. https://doi.org/10.1016/j.istruc.2021.01.052

[11] Xin L, Li X, Zhang Z, Zhao L (2019) Seismic behavior of long-span concrete-flled steel tubular arch bridge subjected to near-fault fing-step motions. Eng Struct 180:148–159. https://doi.org/10.1016/j.engstruct.2018.11.006

[12] Li J, Xu LH. Seismic response characteristics and whiplash effect mechanism of continuous rigid-frame bridges subjected to near-fault ground motions. Bull Earthq Eng 2023; 21: 3719-3744. https://doi.org/10.1007/s10518-023-01672-4

[13]. ECP (2012) - ECP-201, "Egyptian code for calculating loads and forces in structural work and masonry", Housing and Building National Research Centre. Ministry of Housing, Utilities and Urban Planning, Cairo, 2012.

[14] CSiBridge; (2024), Version 26.0.0, Computers and Structures, Inc., CSI Analysis Reference Manual for SAP2000, ETABS, SAFE and CSiBridge. http://www.csiamerica.com/

Figure legend

Table legend